RSC Advances

PAPER

View Article Online
View Journal | View Issue

Cite this: *RSC Adv.*, 2020, **10**, 10420

Structural and thermal properties of $Na_2Mn(SO_4)_2\cdot 4H_2O$ and $Na_2Ni(SO_4)_2\cdot 10H_2O$†

Hamdi Ben Yahia, *[a] Alaa Alkhateeb[a] and Rachid Essehli[b]

The title compounds were prepared *via* a wet chemistry route and their crystal structures were determined from single crystal X-ray diffraction data. $Na_2Mn(SO_4)_2\cdot 4H_2O$ crystallizes with a monoclinic symmetry, space group $P2_1/c$, with $a = 5.5415(2)$, $b = 8.3447(3)$, $c = 11.2281(3)$ Å, $\beta = 100.172(1)°$, $V = 511.05(3)$ Å^3 and $Z = 2$. $Na_2Ni(SO_4)_2\cdot 10H_2O$ also crystallizes with a monoclinic symmetry, space group $P2_1/c$, with $a = 12.5050(8)$, $b = 6.4812(4)$, $c = 10.0210(6)$ Å, $\beta = 106.138(2)°$, $V = 780.17(8)$ Å^3 and $Z = 2$. $Na_2Mn(SO_4)_2\cdot 4H_2O$ is a new member of the blödite family of compounds, whereas $Na_2Ni(SO_4)_2\cdot 10H_2O$ is isostructural with $Na_2Mg(SO_4)_2\cdot 10H_2O$. The structure of $Na_2Mn(SO_4)_2\cdot 4H_2O$ is built up of $[Mn(SO_4)_2(H_2O)_4]^{2-}$ building blocks connected through moderate O–H···O hydrogen bonds with the sodium atoms occupying the large tunnels along the *a* axis and the manganese atom lying on an inversion center, whereas the structure of $Na_2Ni(SO_4)_2\cdot 10H_2O$ is built up of $[Ni(H_2O)_6]^{2+}$ and $[Na_2(SO_4)_2(H_2O)_4]^{2-}$ layers. These layers which are parallel to the (100) plane are interconnected through moderate O–H···O hydrogen bonds. The thermal gravimetric- and the powder X-ray diffraction-analyzes showed that only the nickel phase was almost pure. At a temperature above 300 °C, all the water molecules evaporated and a structural phase transition from $P2_1/c$-$Na_2Ni(SO_4)_2\cdot 10H_2O$ to $C2/c$-$Na_2Ni(SO_4)_2$ was observed. $C2/c$-$Na_2Ni(SO_4)_2$ is thermally more stable than $Na_2Fe(SO_4)_2$ and therefore it would be suitable as the positive electrode for sodium ion batteries if a stable electrolyte at high voltage is developed.

Received 11th January 2020
Accepted 1st March 2020

DOI: 10.1039/d0ra00301h

rsc.li/rsc-advances

1. Introduction

The sulfate salts of general formula $Na_2M(SO_4)_2\cdot nH_2O$ ($n = 1$, 2, 3, 4, 5, 6, 10, 16)[1–14] have attracted much attention from mineralogists during the last century owing to their important role in desertification, soil contamination and surface and ground water salinization [ref. 13 and references therein]. These natural and synthetic sulfate salts crystallize with a wide range of crystal structure types depending on their degree of hydration. This parameter is at the origin of the presence of unique hydrogen bond features in these compounds. For this reason, numerous studies have focused on solving their crystal structures. In the system with magnesium five phases exist. The blödite-type $Na_2Mg(SO_4)_2\cdot 4H_2O$[8] and the konyaite-type $Na_2Mg(SO_4)_2\cdot 5H_2O$[9] are both minerals that form due to the evaporation of saline solutions, whereas $Na_2Mg(SO_4)_2\cdot 10H_2O$[13] and $Na_2Mg(SO_4)_2\cdot 16H_2O$[14] are synthetic phases that were obtained from the evaporation of solutions containing a 1 : 1 molar ratio of $MgSO_4$ and Na_2SO_4 salts. When the same mixture was heated to 650 °C and slow cooled at a rate of 1° min^{-1}, $Na_2Mg(SO_4)_2$ was obtained.[15] The $Na_2M(SO_4)_2\cdot nH_2O$ phases are very sensitive to temperature, pressure and relative humidity. When heated at relatively high temperatures ($T > 200$ °C) these phases could be completely dehydrated to form the $Na_2M(SO_4)_2$ phases which are of interest as positive electrodes for sodium- or lithium-ion batteries.

Among the $Na_2M(SO_4)_2$ phases, $Na_2Fe(SO_4)_2$ showed interesting electrochemical properties in Li- and Na-ion batteries. This phase enables the removal of nearly one sodium at potentials around ~3.6 V *vs.* Li^+/Li or ~3.3 V *vs.* Na^+/Na.[16] $Na_2Fe(SO_4)_2$ could also be obtained by intercalating one sodium into the structure of the eldfellite-type $NaFe(SO_4)_2$.[17] At 0.1C, this material delivers a discharge capacity of 80 mA h g^{-1} with an operating potential around 3.25 V *vs.* Na^+/Na. Even the hydrated phases such as the blödite-type $Na_2Fe(SO_4)_2\cdot 4H_2O$[16] or the kröhnkite-type $Na_2Fe(SO_4)_2\cdot 2H_2O$[18] were active at ~3.3 V and ~3.25 V *vs.* Na^+/Na, respectively. On the other hand, the $Na_2Co(SO_4)_2$ phase did not show any electrochemical activity up to 5 V.[16] In the system $Na_2Mn(SO_4)_2\cdot nH_2O$ two phases were

[a]*Qatar Environment and Energy Research Institute (QEERI 2.0), Hamad Bin Khalifa University, Qatar Foundation, P. O. Box 34110, Doha, Qatar. E-mail: Hyahia@hbku.edu.qa*

[b]*Energy and Transportation Science Division, Oak Ridge National Laboratory, Oak Ridge, TN, USA*

† Electronic supplementary information (ESI) available: The theoretical powder X-ray diffraction patterns (PXRD) of $Na_{12}Mn_7(SO_4)_{13}\cdot 15H_2O$, $Na_2Mn(SO_4)_2\cdot 2H_2O$ and $Na_2Mn(SO_4)_2\cdot 4H_2O$, the experimental PXRD and the TGA of the sample containing manganese and the anisotropic displacement parameters (in Å^2) for $Na_2Mn(SO_4)_2\cdot 4H_2O$ and $Na_2Ni(SO_4)_2\cdot 10H_2O$ are given in supplementary information. CCDC 1962424 and 1962425. For ESI and crystallographic data in CIF or other electronic format see DOI: 10.1039/d0ra00301h

reported ($n = 0$ and 2). The thermal decomposition at 500 K of $Na_2Mn_{1.167}(SO_4)_2S_{0.33}O_{1.167}\cdot 2H_2O$[19] and the kröhnkite-type $Na_2Mn(SO_4)_2\cdot 2H_2O$[20] led to the formation of two different $Na_2Mn(SO_4)_2$ phases that crystallize with the glauberite- and alluaudite-type of structures, respectively. The glauberite-type $Na_2Mn(SO_4)_2$ sample was not tested as positive electrode since it contains few MnS_2O_7 impurities and the alluaudite-type $Na_2Mn(SO_4)_2$ has shown to be active in sodium ion batteries (NIBs), however the performance was worse than the iron analogues.[21–23] In the system $Na_2Ni(SO_4)_2\cdot nH_2O$ three phases are known ($n = 0$, 4 and 6), however they were not tested as positive electrode materials for NIBs.[24–26] For these reasons we prepared recently several $Na_2M(SO_4)_2\cdot nH_2O$ phases (M = Mn and Ni) in order to test their electrochemical performances in NIBs.

In this paper we report on the synthesis of the new phases $Na_2Mn(SO_4)_2\cdot 4H_2O$ and $Na_2Ni(SO_4)_2\cdot 10H_2O$ by wet chemistry route. The crystal structures of these phases were solved using single crystal X-ray diffraction (XRD) and their compositions were confirmed by the combination of thermal gravimetric analyzes (TGA) and energy-dispersive X-ray spectrometry analyzes (EDX). The fully dehydrated phases were analyzed by *ex situ* powder XRD. Our results are presented in the following sections.

2. Experimental section

2.1. Synthesis

$Na_2Mn(SO_4)_2\cdot 4H_2O$ powder was synthesized *via* a wet chemistry route (super-saturation method) from a stoichiometric mixture of Na_2SO_4 (Aldrich, ≥99%) and $MnSO_4\cdot H_2O$ (Aldrich, ≥99%). The starting materials with a 1 : 1 molar ratio were dissolved in 20 ml of water (solution A). The solution A was stirred for few hours then left drying at room temperature during four weeks. This enabled the growth of a mixture of large colorless single crystals of $Na_{12}Mn_7(SO_4)_{13}\cdot 15H_2O$, $Na_2Mn(SO_4)_2\cdot 2H_2O$ and the new phase $Na_2Mn(SO_4)_2\cdot 4H_2O$. Powder sample of this sample was obtained by grinding few crystals.

$Na_2Ni(SO_4)_2\cdot 10H_2O$ powder was also synthesized *via* a wet chemistry route (super-saturation method) from a stoichiometric mixture of Na_2SO_4 (Aldrich, ≥99%) and $NiSO_4\cdot 6H_2O$ (Aldrich, ≥99%). The starting materials with a 1 : 1 molar ratio were dissolved in 20 ml of water (solution B). The solution B was stirred for few hours then left drying at room temperature during three weeks. This enabled the growth of large green single crystals of the new phase $Na_2Ni(SO_4)_2\cdot 10H_2O$. Powder sample of this material was obtained by grinding few crystals. The solution B was also dried at 80 °C for 12 hours then the resulting powder was grinded and fired at 350 °C for 32 hours. This led to the formation of the green powder of SS-$Na_2Ni(SO_4)_2$. A similar powder of WC-$Na_2Ni(SO_4)_2$ was obtained when heating under argon the crystals of $Na_2Ni(SO_4)_2\cdot 10H_2O$ at 400 °C for 6 hours.

2.2. Powder X-ray diffraction measurements

To ensure the purity of the prepared powders, routine powder XRD measurements were performed. The data were collected at room temperature over the 2θ angle range of $5° \le 2\theta \le 75°$ with a step size of 0.01° using a Bruker D8 advance diffractometer operating with CuKα radiation. Full pattern matching refinement was performed with the JANA2006 program package.[27] The background was estimated by a Legendre function and the peak shapes were described by a pseudo-Voigt function.

2.3. Single crystal X-ray diffraction measurements

$Na_2Mn(SO_4)_2\cdot 4H_2O$ and $Na_2Ni(SO_4)_2\cdot 10H_2O$ single crystals suitable for single crystal X-ray diffraction were selected on the basis of the size and the sharpness of the diffraction spots. The data collections were carried out on a Bruker D8 Venture diffractometer using MoKα radiation. Data processing and all refinements were performed with the APEX3 and JANA2006 program packages, respectively.[27,28] For the data collection details, see Table 1. Further details on the structure refinements of $Na_2Mn(SO_4)_2\cdot 4H_2O$ and $Na_2Ni(SO_4)_2\cdot 10H_2O$ may be obtained from the Fachinformationszentrum Karlsruhe, D-76344 Eggenstein-Leopoldshafen (Germany), by quoting the Registry No. CSD – 1962424 and 1962425.

2.4. Electron microprobe analyzes

Semi-quantitative energy-dispersive X-ray spectrometry (EDX) analyzes were carried out on the single crystals used for the data collections with a 7610F (JEOL) scanning electron microscope (SEM). The experimentally observed Na/M/S atomic ratios (M = Mn and Ni) were close to 2 : 1 : 2, as expected for $Na_2Mn(SO_4)_2\cdot 4H_2O$ and $Na_2Ni(SO_4)_2\cdot 10H_2O$.

2.5. Thermal analyzes

Thermal gravimetric analyzes (TGA) were carried out on the prepared samples $Na_2Mn(SO_4)_2\cdot 4H_2O$ and $Na_2Ni(SO_4)_2\cdot 10H_2O$ using a TA-SDT 650 instrument. The measurements were conducted between 25 and 850 °C at a heating rate of 10 °C min^{-1}. The experiments were performed in alumina crucible under N_2 atmosphere.

3. Results and discussion

3.1. Structure refinement

The systematic absences observed for $Na_2Mn(SO_4)_2\cdot 4H_2O$ and $Na_2Ni(SO_4)_2\cdot 10H_2O$ agree with the space group $P2_1/c$. Atomic positions of the majority of atoms were found by the Superflip program implemented in JANA2006 program package.[27,29] The use of the difference Fourier synthesis allowed us to localize the remaining oxygen atomic positions. With anisotropic atomic displacement parameters (ADPs), the residual factors converged to the value $R(F) = 0.0264$ and $wR(F^2) = 0.0949$ (G.O.F. = 1.92) for 79 refined parameters and 1198 observed reflections for the compound $Na_2Mn(SO_4)_2\cdot 4H_2O$ and $R(F) = 0.0345$ and $wR(F^2) = 0.1165$ (G.O.F. = 1.92) for 106 refined parameters and 2781 observed reflections for the compound $Na_2Ni(SO_4)_2\cdot 10H_2O$. At this stage of the refinements the chemical formulas were $Na_2Mn(SO_4)_2\cdot 4O$ and $Na_2Ni(SO_4)_2\cdot 10O$. The H atomic positions were determined from the difference-Fourier maps. The O–H distances and H–O–H angles were set to 0.96 Å and 104.5°,

Table 1 Crystallographic data and structure refinements for $Na_2Mn(SO_4)_2\cdot 4H_2O$ and $Na_2Ni(SO_4)_2\cdot 10H_2O$

Crystal data		
Chemical formula	$Na_2Mn(SO_4)_2\cdot 4H_2O$	$Na_2Ni(SO_4)_2\cdot 10H_2O$
M_r	365.1	476.9
Crystal system, space group	Monoclinic, $P2_1/c$	Monoclinic, $P2_1/c$
Temperature (K)	293	293
a, b, c (Å)	5.5415 (2), 8.3447 (3), 11.2281 (3)	12.5050 (8), 6.4812 (4), 10.0210 (6)
β (°)	100.172 (1)	106.138 (2)
V (Å^3)	511.05 (3)	780.17 (8)
Z	2	2
Radiation type	Mo Kα	Mo Kα
μ (mm^{-1})	1.84	1.66
Crystal size (mm)	0.16 × 0.13 × 0.11	0.34 × 0.10 × 0.08
Data collection		
Diffractometer	Bruker D8 VENTURE	Bruker D8 VENTURE
Absorption correction	Multi-scan (SADABS)	Multi-scan SADABS
T_{min}, T_{max}	0.88, 0.92	0.630, 0.747
No. of measured, independent and observed [$I > 3\sigma(I)$] reflections	9618, 1314, 1198	22 158, 3819, 2781
R_{int}	0.022	0.029
$(\sin\theta/\lambda)_{max}$ (Å^{-1})	0.676	0.853
Refinement		
$R[F^2 > 2\sigma(F^2)]$, w$R(F^2)$, S	0.018, 0.060, 1.16	0.024, 0.079, 1.11
No. of reflections	1314	3819
No. of parameters	96	147
No. of restraints	6	15
H-atom treatment	All H-atom parameters refined	All H-atom parameters refined
$\Delta\rho_{max}$, $\Delta\rho_{min}$ (e Å^{-3})	0.19, −0.23	0.33, −0.33

respectively. The U_{iso}(H) were refined without constrains. This led to the final chemical formula $Na_2Mn(SO_4)_2\cdot 4H_2O$ with the residual factors $R(F) = 0.0198$ and w$R(F^2) = 0.0629$ (G.O.F. = 1.22 for 95 refined parameters) and the chemical formula $Na_2Ni(SO_4)_2\cdot 10H_2O$ with the residual factors $R(F) = 0.0251$ and w$R(F^2) = 0.0707$ (G.O.F. = 1.18 for 146 refined parameters). By refining the extinction parameters, the residual factors converged to the values given in Table 1. The refined atomic positions and anisotropic ADPs are given in Tables 2 and S1,† respectively. The EDX elemental analyzes performed on the crystals used for the data collection confirmed the compositions $Na_2Mn(SO_4)_2\cdot xH_2O$ and $Na_2Ni(SO_4)_2\cdot xH_2O$ (Fig. 1). The examination of the powder XRD pattern of the manganese sample revealed the presence of mainly $Na_{12}Mn_7(SO_4)_{13}\cdot 15H_2O$[30] besides a small amount of $Na_2Mn(SO_4)_2\cdot 2H_2O$[2] and $Na_2Mn(SO_4)_2\cdot 4H_2O$ (Fig. S1†), whereas the nickel sample was almost a pure $Na_2Ni(SO_4)_2\cdot 10H_2O$ phase. Fig. 2 shows a good agreement between the experimental and calculated patterns of $Na_2Ni(SO_4)_2\cdot 10H_2O$. Evaluation of these data revealed the refined cell parameters $a = 12.4926(5)$, $b = 6.4763(2)$, $c = 10.0153(4)$ Å and $\beta = 106.070(2)°$ which are in good agreement with those from single crystal diffraction data (see Table 1). Only three tiny impurity peaks were detected. The composition of the $Na_2Ni(SO_4)_2\cdot 10H_2O$ sample was confirmed by the combination of EDX (Fig. 1b) and TGA analyzes.

Fig. 3 clearly indicates a 37.7% of weight loss, which corresponds exactly to the evaporation of ten water molecules. This confirms that the prepared sample $Na_2Ni(SO_4)_2\cdot 10H_2O$ decomposes below 300 °C to form WC-$Na_2Ni(SO_4)_2$ according to the following scheme:

$$Na_2Ni(SO_4)_2\cdot 10H_2O_{(s)}\ (476.95\ g\ mol^{-1}) \rightarrow WC\text{-}Na_2Ni(SO_4)_{2(s)}\ (296.8\ g\ mol^{-1}) + 10H_2O_{(g)}\ (180.15\ g\ mol^{-1})$$

This decomposition mechanism was confirmed by powder XRD, since the powder pattern of the dehydrated $Na_2Ni(SO_4)_2\cdot 10H_2O$ phase is identical to the theoretical pattern of $Na_2Ni(SO_4)_2$ and the experimental pattern of SS-$Na_2Ni(SO_4)_2$ (Fig. 4). Above 700 °C, the sample decomposes by releasing $SO_{2(g)}$. It should be noted that the thermal behavior of the sample containing manganese was also performed (Fig. S2†). The weight loss was only 12.9% which is lower than the weight loss of 19.7% expected for $Na_2Mn(SO_4)_2\cdot 4H_2O$, however it is almost identical to the weight loss of 12.4% expected for $Na_{12}Mn_7(SO_4)_{13}\cdot 15H_2O$. This is in good agreement with PXRD data which indicate that the prepared manganese phase contains mainly the $Na_{12}Mn_7(SO_4)_{13}\cdot 15H_2O$ phase.

3.2. Crystal structure of $Na_2Mn(SO_4)_2\cdot 4H_2O$

The $Na_2Mn(SO_4)_2\cdot 4H_2O$ compound is isostructural with the blödite-type compounds $Na_2M(SO_4)_2\cdot 4H_2O$ (M = Mg, Fe, Co, Ni, Zn, Cd).[31–37] Conventionally, the blödite-type of structure is described as a stacking of layers parallel to the (010) plane and formed of $MnO_2(H_2O)_4$ and $NaO_4(H_2O)_2$ octahedra (Fig. 5a and b). These layers are interconnected through SO_4 tetrahedra to form a 3d-framework (Fig. 5c). The interatomic distances are listed in Table 3.

Table 2 Fractional atom coordinates and isotropic atomic displacement parameters (Å^2) for $Na_2Mn(SO_4)_2\cdot 4H_2O$ and $Na_2Ni(SO_4)_2\cdot 10H_2O$

Atom	Wyck	x	y	z	U_{eq}/iso*
$Na_2Mn(SO_4)_2\cdot 4H_2O$					
Na1	4e	0.12901(9)	0.92766(6)	0.36268(5)	0.02082(16)
Mn1	2a	0	0.5	0.5	0.01387(10)
S1	4e	0.37292(5)	0.79212(3)	0.63561(2)	0.01132(10)
O1	4e	0.20851(18)	0.91681(12)	0.57815(8)	0.0234(3)
O2	4e	0.31892(17)	0.63864(11)	0.57209(9)	0.0233(3)
O3	4e	0.63145(16)	0.83269(11)	0.63209(9)	0.0222(3)
O4	4e	0.34724(18)	0.77406(12)	0.76397(8)	0.0216(3)
O5	4e	0.13017(16)	0.45884(12)	0.33232(8)	0.0181(3)
H5b	4e	0.232(3)	0.3650(13)	0.3423(18)	0.040(5)*
H5a	4e	0.235(3)	0.5421(17)	0.312(2)	0.053(6)*
O6	4e	0.18486(17)	0.28225(10)	0.58278(8)	0.0192(3)
H6a	4e	0.223(3)	0.210(2)	0.5222(13)	0.053(7)*
H6b	4e	0.3331(17)	0.288(2)	0.6416(12)	0.039(5)*
$Na_2Ni(SO_4)_2\cdot 10H_2O$					
Na1	4e	0.48096(4)	0.25441(7)	0.39586(5)	0.02511(14)
Ni1	2c	1.00000	0	1/2	0.01379(6)
S1	4e	0.72260(2)	0.51630(3)	0.33017(3)	0.01445(7)
O1	4e	0.79184(6)	0.42137(12)	0.24800(9)	0.0233(2)
O2	4e	0.78000(8)	0.49977(11)	0.48001(9)	0.0234(3)
O3	4e	0.61500(7)	0.41153(15)	0.29742(9)	0.0296(3)
O4	4e	0.70453(7)	0.73541(11)	0.29108(9)	0.0254(2)
O5	4e	0.86644(7)	0.03383(11)	0.33044(10)	0.0247(2)
H5a	4e	0.8331(9)	0.1634(11)	0.3001(15)	0.036(4)*
H5b	4e	0.8058(7)	−0.0615(16)	0.309(2)	0.057(5)*
H6a	4e	0.9914(11)	0.294(3)	0.6835(6)	0.064(6)*
H6b	4e	0.9025(7)	0.342(2)	0.5531(12)	0.029(4)*
O6	4e	0.97063(7)	0.27252(11)	0.58560(8)	0.0239(2)
O7	4e	0.60084(7)	0.40809(12)	0.60325(9)	0.0250(2)
H7a	4e	0.6193(11)	0.314(2)	0.6794(13)	0.059(5)*
H7b	4e	0.6698(7)	0.435(2)	0.5838(18)	0.057(5)*
O8	4e	0.38581(8)	0.03475(14)	0.52844(10)	0.0287(3)
H8a	4e	0.3566(12)	0.123(3)	0.5863(16)	0.068(6)*
H8b	4e	0.3216(8)	−0.023(2)	0.4645(15)	0.050(6)*
O9	4e	0.90973(6)	−0.16068(11)	0.61345(8)	0.0219(2)
H9a	4e	0.8634(10)	−0.085(2)	0.6567(16)	0.044(5)*
H9b	4e	0.8662(11)	−0.2770(18)	0.5734(19)	0.059(5)*

The manganese atom is lying on an inversion center and is coordinated to two oxygen atoms and four water molecules forming $[MnO_2(H_2O)_4]^{2-}$ octahedron. This octahedron share corners with two SO_4 tetrahedra forming the building block $[Mn(SO_4)_2(H_2O)_4]^{2-}$ (Fig. 5e). The $[MnO_2(H_2O)_4]^{2-}$ octahedron share also corners with four $[Na_2O_6(H_2O)_4]^{10-}$ dimer units leading to layers in the (010) plane (Fig. 5a). The $d_{(Mn1-O)}$ distances range from 2.1475 to 2.2088 Å with an average distance of 2.1718 Å which is slightly shorter than the sum of the effective ionic radii of the six-coordinated Mn^{2+} and O^{2-} {$IR_{(Mn^{2+})} + IR_{(O^{2-})} = 0.83 + 1.4$ Å}.[38] The BVS value of 2.14 is in good agreement with the oxidation state 2+ expected for the Mn atoms.[39]

The slightly distorted SO_4 tetrahedra share only corners with the $MnO_2(H_2O)_4$ and $NaO_4(H_2O)_2$ octahedra (Fig. 5c). The $d_{(S1-O)}$ distances range from 1.4565 to 1.4807 Å with the average value of 1.4718 Å. This value is shorter than the sum of the effective ionic radii of the four-coordinated S^{6+} and O^{2-} {$IR_{(S^{6+})} + IR_{(O^{2-})} =$ 0.12 + 1.38 Å}. The BVS value of 6.03 is in good agreement with the oxidation state 6+ expected for sulfur.

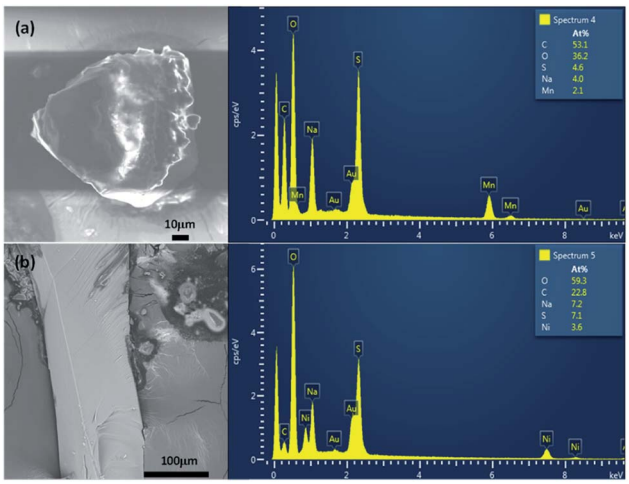

Fig. 1 Images and EDX analyzes of $Na_2Mn(SO_4)_2\cdot 4H_2O$ (a) and $Na_2Ni(SO_4)_2\cdot 10H_2O$ (b). These are the single crystals used for the data collections.

The sodium atom is coordinated to four oxygen atoms and two water molecules forming $[NaO_4(H_2O)_2]^{7-}$ octahedra. These octahedra share edges and form $[Na_2O_6(H_2O)_4]^{10-}$ dimer units (Fig. 5f). The average Na1–O distance of 2.4528 Å is consistent with the sum of the effective ionic radii of the six-coordinated Na^+ and O^{2-} {$IR_{(Na^+)} + IR_{(O^{2-})} = 1.02 + 1.40$ Å}. The BVS value of 1.06 is in good agreement with the oxidation state 1+ expected for the Na atoms.

In the crystal structure of $Na_2Mn(SO_4)_2\cdot 4H_2O$, the H_2O molecules play the role of hydrogen-bond donors whereas the oxygen atoms O3 and O4 are the hydrogen bond acceptors (Table 4 and Fig. 6). The O–H···O hydrogen bonds connect the $[Mn(SO_4)_2(H_2O)_4]^{2-}$ building blocks (Fig. 5e) forming a tunnel-like structure with large voids along the *a* axis (Fig. 6a). In these voids, the sodium atoms are located (Fig. 5d and 6a). This feature indicates that the compounds of the blödite-family might be good ionic conductors. This may explain the electrochemical activity of the $Na_2Fe(SO_4)_2\cdot 4H_2O$ phase in NIBs and LIBs.[16] Based on the classification of Jeffrey, all the O–H···O hydrogen bonds are moderate (Table 4 and Fig. 6b and c).[40,41]

It is very interesting to notice that the manganese phases $Na_2Mn(SO_4)_2\cdot 4H_2O$ [this work], $Na_2Mn(SO_4)_2\cdot 2H_2O$,[20] $Na_{2+\gamma}Mn_{1-\gamma/2}(SO_4)_3$,[20] $Na_{12}Mn_7(SO_4)_{12}[S_2O_7]\cdot 12H_2O$[19] and $Na_2Mn(SO_4)_2$ [19] that crystallize with the blödite-, kröhnkite-, alluaudite-, löweite- and glauberite-type of structures, respectively were prepared *via* a supersaturation method at different temperatures and using the same precursors (Na_2SO_4 + $MnSO_4\cdot H_2O$ + H_2O). At 25 and 70 °C, pure kröhnkite- and löweite-phases were formed, respectively whereas at 22 °C a mixture of kröhnkite-, blödite- and löweite-phases was observed. Furthermore, the thermal treatment of the kröhnkite-phase at 227 °C, led to the formation of an alluaudite-phase with the composition $Na_{2+\gamma}Mn_{1-\gamma/2}(SO_4)_3$.[20] A similar phase could also be prepared *via* a solid state synthesis route when a mixture of Na_2SO_4 and $MnSO_4$ was

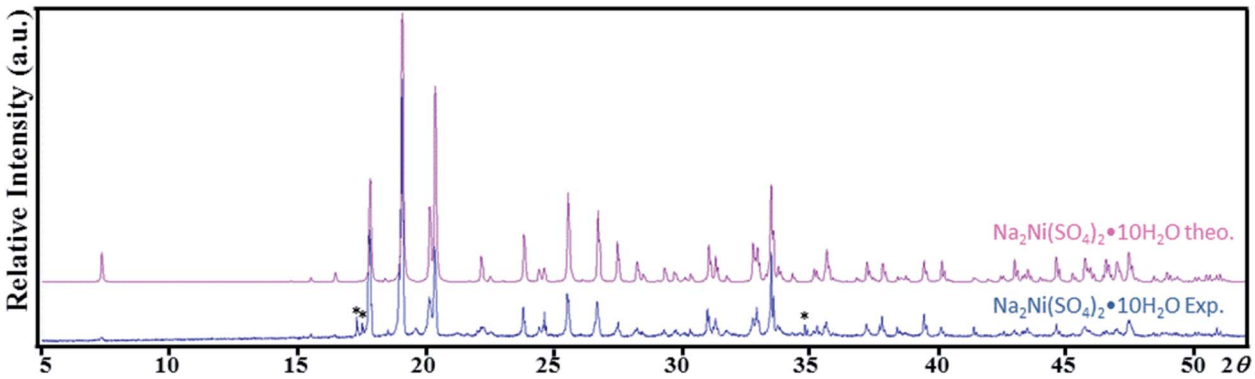

Fig. 2 Theoretical and experimental powder X-ray diffraction patterns of $Na_2Ni(SO_4)_2 \cdot 10H_2O$ (Cu-Kα radiation). Asterisk (*) corresponds to an unidentified impurity.

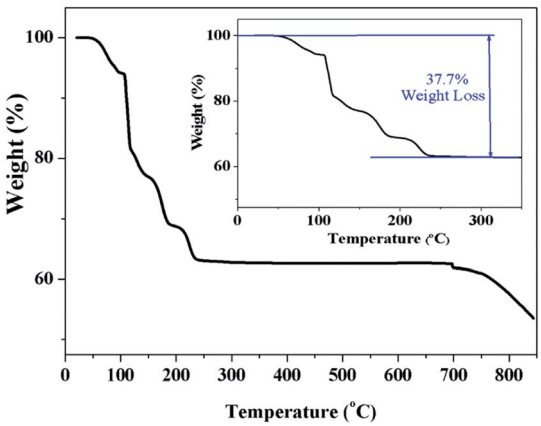

Fig. 3 TGA thermal analysis of the $Na_2Ni(SO_4)_2 \cdot 10H_2O$ sample.

ball milled then annealed at 350 °C for few hours.[42] Moreover, at 227 °C the löweite-phase decomposed into the glauberite-phase $Na_2Mn(SO_4)_2$ besides an impurity that could be MnS_2O_7.[19] Although, the five phases were prepared from the same precursors, their crystal structures are different (Fig. 7). Indeed, the thermal treatments affected significantly the coordination sphere of the Mn atoms. In the blödite-$Na_2Mn(SO_4)_2 \cdot 4H_2O$, the Mn atom is coordinated to two oxygen atoms and four water molecules forming the $[MnO_2(H_2O)_4]^{2-}$ octahedron. This octahedron share two corners with the SO_4 tetrahedra to form the $[Mn(SO_4)_2(H_2O)_4]^{2-}$ building block (Fig. 7a). In the kröhnkite-$Na_2Mn(SO_4)_2 \cdot 2H_2O$, the Mn atom is coordinated to four oxygen atoms and two water molecules. The MnO_6 octahedra share corners with four SO_4 tetrahedra to form infinite chains along the *c* axis (Fig. 7b). These chains are condensed at 227 °C to form the 3d-framework of the alluaudite-$Na_{2+\gamma}Mn_{1-\gamma/2}(SO_4)_3$. In this structure the MnO_6 octahedra share edges and form dimer units that are interconnected through SO_4 tetrahedra (Fig. 7c). In the löweite-$Na_{12}Mn_7(SO_4)_{12}[S_2O_7] \cdot 12H_2O$, two Mn atoms exist. Mn1 is coordinated to two water molecules and four oxygen atoms, whereas Mn2 is coordinated to six oxygen atoms. The $Mn1O_6$ and $Mn2O_6$ octahedra are bridged by the SO_4 tetrahedra to form a 3d-framework (Fig. 7d). At 227 °C, the water molecules of the löweite evaporated and

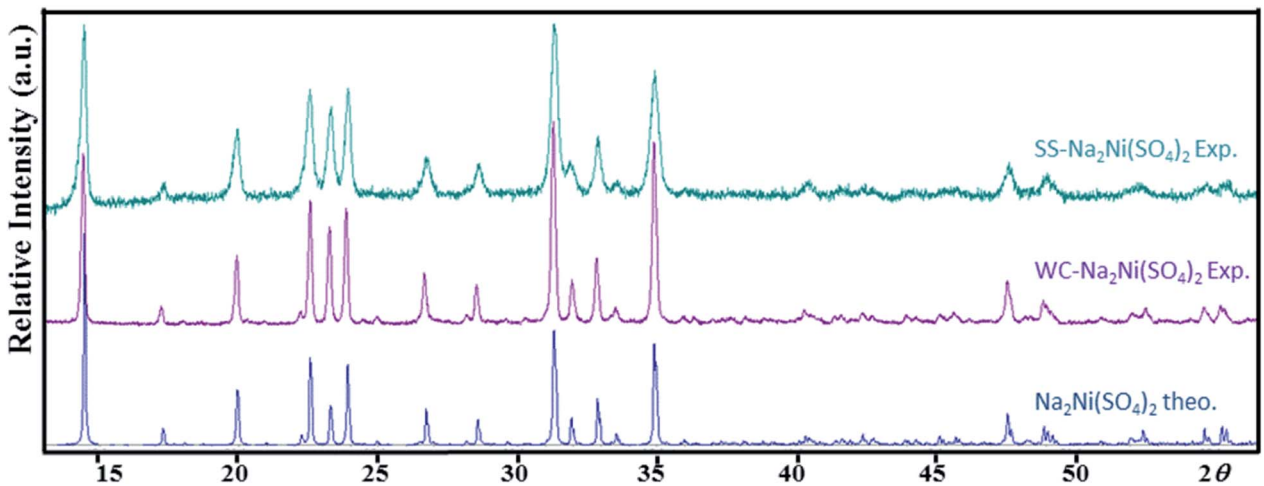

Fig. 4 Theoretical and experimental powder X-ray diffraction patterns of $Na_2Ni(SO_4)_2$ (Cu-Kα radiation). SS-$Na_2Ni(SO_4)_2$ was obtained using solid state synthesis method, whereas WC-$Na_2Ni(SO_4)_2$ corresponds to the dehydration of $Na_2Ni(SO_4)_2 \cdot 10H_2O$ obtained using wet chemistry route.

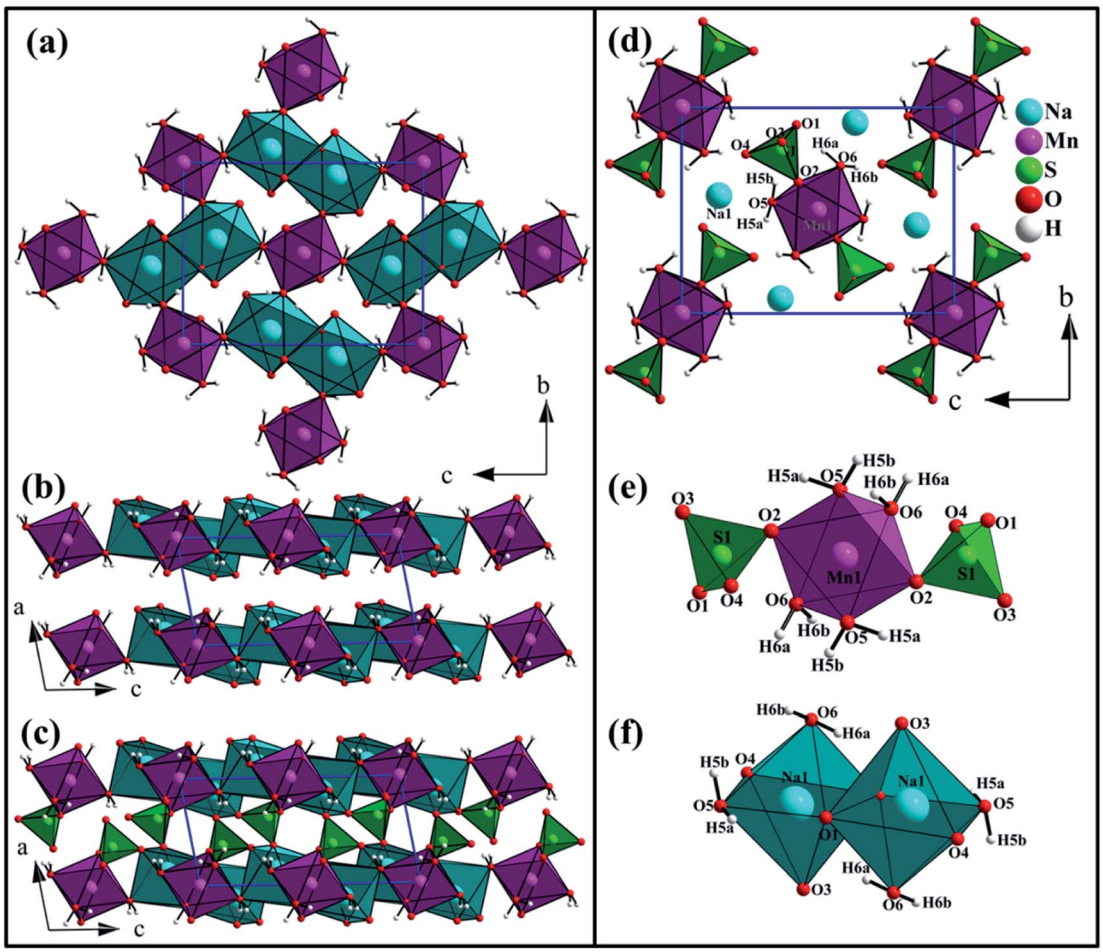

Fig. 5 View along the *a* and *b* axes of the layers of $MnO_2(H_2O)_4$ and $NaO_4(H_2O)_2$ octahedra (a and b), and projection view of the crystal structure of $Na_2Mn(SO_4)_2\cdot 4H_2O$ in the (010) plane (c). View along the *a* axis of the crystal structure of $Na_2Mn(SO_4)_2\cdot 4H_2O$ (d). The atoms of the asymmetric unit are labeled (d). View of the building block $[Mn(SO_4)_2(H_2O)_4]^{2-}$ (e) and the $[Na_2O_6(H_2O)_4]^{10-}$ dimer units (f).

a structural transition to the glauberite-$Na_2Mn(SO_4)_2$ was observed. In this structure the MnO_6 octahedra share corners with six SO_4 tetrahedra to form a 3d-framework (Fig. 7e).

3.3. Crystal structure of $Na_2Ni(SO_4)_2\cdot 10H_2O$

The $Na_2Ni(SO_4)_2\cdot 10H_2O$ compound is isostructural with $Na_2Mg(SO_4)_2\cdot 10H_2O$.[12] The structure is built up of $[Ni(H_2O)_6]^{2+}$ and $[Na_2(SO_4)_2(H_2O)_4]^{2-}$ layers parallel to the (100) plane. These layers are interconnected through hydrogen bonds forming the structure of $Na_2Ni(SO_4)_2\cdot 10H_2O$. The interatomic distances and the hydrogen bonds are listed in Tables 3 and 4, respectively.

The nickel cations are coordinated to six water molecules forming isolated distorted $[Ni(H_2O)_6]^{2+}$ octahedra. These octahedra are interlinked by the O6–H6a···O9 hydrogen bonds forming the layer 2 parallel to the (100) plane (Fig. 8c). The $d_{(Ni1-O)}$ distances range from 2.0365 to 2.0892 Å with an average distance of 2.0555 Å which is slightly shorter than the sum of the effective ionic radii of the six-coordinated Ni^{2+} and O^{2-} $\{IR_{(Ni^{2+})} + IR_{(O^{2-})} = 0.69 + 1.4$ Å$\}$.[38] The BVS value of 2.03 is in good agreement with the oxidation state 2+ expected for the Ni atoms.[39]

The SO_4 tetrahedra are regular. The distances range from 1.4607 to 1.4842 Å with the average value of 1.4740 Å. This value is shorter than the sum of the effective ionic radii of the four-coordinated S^{6+} and O^{2-} $\{IR_{(S^{6+})} + IR_{(O^{2-})} = 0.12 + 1.38$ Å$\}$. The BVS value of 6.00 is in good agreement with the oxidation state 6+ expected for sulfur.

The $Na1^+$ cations are surrounded by six oxygen atoms forming distorted octahedra. These octahedra share edges and form infinite chains running along the *b* axis (Fig. 8b). These chains share corners with the SO_4 tetrahedra forming $[Na_2(SO_4)_2(H_2O)_4]^{2-}$ layers parallel to the (100) plane (see layer 1 in Fig. 8b). The average Na1–O distance of 2.4537 Å is consistent with the sum of the effective ionic radii of the six-coordinated Na^+ and O^{2-} $\{IR_{(Na^+)} + IR_{(O^{2-})} = 1.02 + 1.40$ Å$\}$. The BVS value of 1.04 is in good agreement with the oxidation state 1+ expected for the Na atoms.

In $Na_2Ni(SO_4)_2\cdot 10H_2O$ the water molecules are the hydrogen-bond donors, whereas the oxygen atoms O1, O3, O3, O4 and O9 play the role of hydrogen bond acceptors (Table 4 and Fig. 9).

Table 3 Interatomic distances (in Å) and bond valence sums (BVS) for $Na_2Mn(SO_4)_2\cdot 4H_2O$ and $Na_2Ni(SO_4)_2\cdot 10H_2O$[a]

	Distances (Å)		Distances (Å)
$Na_2Mn(SO_4)_2\cdot 4H_2O$		**$Na_2Ni(SO_4)_2\cdot 10H_2O$**	
Na1–O1	2.3831(10)	Na1–O3	2.3956(11)
Na1–O3	2.3952(11)	Na1–O4	2.5474(9)
Na1–O5	2.4111(9)	Na1–O7	2.4138(9)
Na1–O4	2.4490(11)	Na1–O7	2.4159(9)
Na1–O1	2.4623(12)	Na1–O8	2.4671(12)
Na1–O6	2.6162(11)	Na1–O8	2.4821(10)
$\langle d_{Na1-O}\rangle$	⟨2.4528⟩	$\langle d_{Na1-O}\rangle$	⟨2.4537⟩
BVS	[b]1.06[6]	BVS	[b]1.04[6]
Mn1–O2 (×2)	2.1475(9)	Ni1–O5 (×2)	2.0365(8)
Mn1–O5 (×2)	2.1593(9)	Ni1–O6 (×2)	2.0409(8)
Mn1–O6 (×2)	2.2088(9)	Ni1–O9 (×2)	2.0892(9)
$\langle d_{Mn1-O}\rangle$	⟨2.1718⟩	$\langle d_{Ni1-O}\rangle$	⟨2.0555⟩
BVS	[b]2.14[6]	BVS	[b]2.03[6]
S1–O1	1.4565(10)	S1–O1	1.4842(10)
S1–O2	1.4707(10)	S1–O2	1.4772(9)
S1–O3	1.4794(9)	S1–O3	1.4607(9)
S1–O4	1.4807(10)	S1–O4	1.4738(7)
$\langle d_{S1-O}\rangle$	⟨1.4718⟩	$\langle d_{S1-O}\rangle$	⟨1.4740⟩
BVS	[b]6.03[4]	BVS	[b]6.00[4]

[a] Average distances are given in ⟨ ⟩ and coordination numbers are given in [ ]. [b] Bond valence sum, B.V. $= e^{(r_0-r)/b}$ with the following parameters: $b = 0.37$, r_0 (Na^{I}–O) = 1.803, r_0 (S^{VI}–O) = 1.624, r_0 (Ni^{II}–O) = 1.654 and r_0 (Mn^{II}–O) = 1.624.

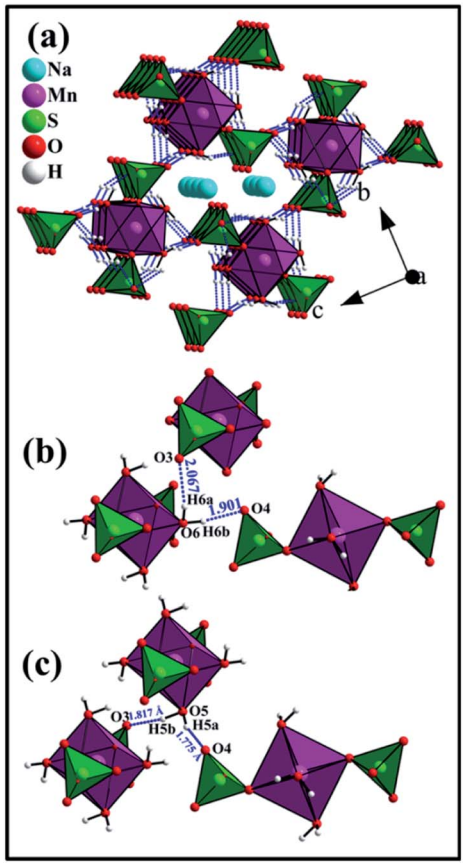

Fig. 6 Perspective view along the *a* axis of the crystal structure of $Na_2Mn(SO_4)_2\cdot 4H_2O$ (a). The dashed blue lines correspond to the O–H···O hydrogen bonds interconnecting the $[Mn(SO_4)_2(H_2O)_4]^{2-}$ building blocks involving the water molecules H6a–O6–H6b (b) and H5a–O5–H5b (c). The sodium atoms are located in the tunnels (a).

The hydrogen bonds can be divided into two categories; intra- and inter-layers bonds as depicted on Fig. 9a, c and b, respectively. Based on the classification of Jeffrey all the O–H···O hydrogen bonds are moderate (Table 4 and Fig. 9).[40,41]

It is worth to mention that in the nickel system $Na_2Ni(SO_4)_2\cdot nH_2O$ four phases have been reported (n = 0, 2, 4 and 6), however only the crystal structures of $Na_2Ni(SO_4)_2$,[24] $Na_2Ni(SO_4)_2\cdot 4H_2O$[25] and $Na_2Ni(SO_4)_2\cdot 6H_2O$[26] were solved (Fig. 10). Theses phases were prepared *via* solid state-, room temperature- and hydrothermal-synthesis routes, respectively and using different precursors and solvents. These experimental conditions are at the origin of the variation in the degree of hydration n of the $Na_2Ni(SO_4)_2\cdot nH_2O$ phases which induced several

Table 4 Hydrogen bonds for $Na_2Mn(SO_4)_2\cdot 4H_2O$ and $Na_2Ni(SO_4)_2\cdot 10H_2O$

Donor	Hydrogen	Acceptor	D–H distance	H···A distance	D–A distance	A–H···D angle
$Na_2Mn(SO_4)_2\cdot 4H_2O$						
O5	H5b	O3	0.960(13)	1.817(12)	2.7634(13)	168.3(15)
O5	H5a	O4	0.960(17)	1.774(16)	2.7074(14)	163.3(14)
O6	H6a	O3	0.960(17)	2.067(16)	2.9400(14)	150.4(16)
O6	H6b	O4	0.960(10)	1.901(10)	2.8483(12)	168.8(13)
$Na_2Ni(SO_4)_2\cdot 10H_2O$						
O5	H5a	O1	0.949(8)	1.785(8)	2.7263(11)	171.2(10)
O5	H5b	O4	0.955(9)	1.800(10)	2.7480(11)	171.0(13)
O6	H6a	O9	0.952(6)	2.088(7)	3.0022(11)	160.5(12)
O6	H6b	O2	0.939(10)	1.817(10)	2.7512(11)	172.9(11)
O7	H7a	O3	0.955(13)	1.888(14)	2.8137(12)	162.4(12)
O7	H7b	O2	0.952(12)	1.988(15)	2.9045(14)	160.9(13)
O8	H8a	O4	0.955(17)	1.861(17)	2.8111(14)	172.9(15)
O8	H8b	O1	0.952(11)	2.236(13)	3.1189(11)	153.7(13)
O9	H9a	O1	0.950(15)	1.795(15)	2.7389(12)	172.3(11)
O9	H9b	O2	0.951(12)	1.889(13)	2.8384(10)	175.4(17)

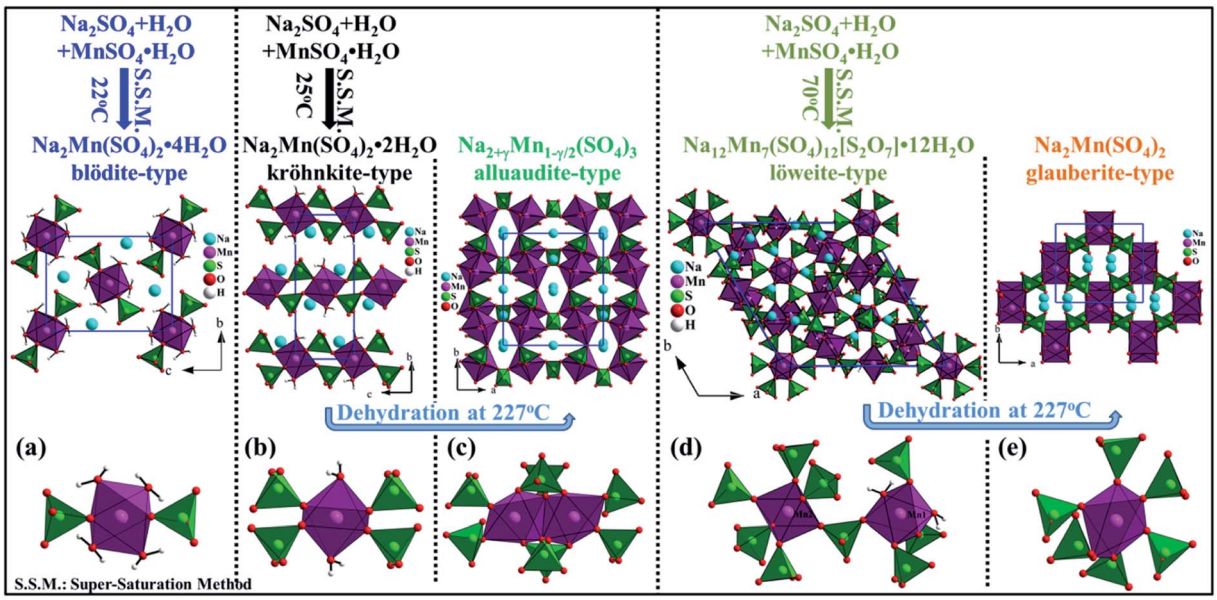

Fig. 7 Synthesis methods and crystal structure views for $Na_2Mn(SO_4)_2\cdot 4H_2O$ (a), $Na_2Mn(SO_4)_2\cdot 2H_2O$ (b), $Na_{2+\gamma}Mn_{1-\gamma/2}(SO_4)_3$ (c), $Na_{12}Mn_7(SO_4)_{12}[S_2O_7]\cdot 12H_2O$ (d) and $Na_2Mn(SO_4)_2$ (e). The coordination spheres of the Mn atoms are also provided for comparison.

structural changes. Our careful analyses indicate that the presence of water molecules affects in first place the coordination sphere of the transition metal (nickel) due to its large electrical charge z. Indeed, for $n = 0$, the NiO_6 octahedra share one edge and four corners with five SO_4 tetrahedra leading to $[Ni(SO_4)_2]^{2-}$ 3d-framework (Fig. 10d). Whereas, for $n = 4$, the Ni atoms are coordinated to four water molecules and two oxygen atoms, from two adjacent SO_4 tetrahedra, forming the isolated $[Ni(SO_4)_2(H_2O)_4]^{2-}$ building block of the blödite-type of structure (Fig. 10a). For $n = 6$ and 10, six water molecules are coordinated to the Ni atoms forming the isolated $[Ni(H_2O)_6]^{2+}$ octahedra (Fig. 10b and c) which are connected to the SO_4 tetrahedra only through hydrogen bonds. For $n = 10$, the $(n - 6)$ extra water molecules are coordinated to the sodium atoms. Since $n \leq 10$, in the four phases the water molecules are coordinated. One would expect to observe interstitial water only for $n > 12$. Indeed in the case of $Na_2Mg(SO_4)_2\cdot 16H_2O$, six water molecules are coordinated to the magnesium atoms, six water molecules are coordinated to the sodium atoms and four water molecules are interstitial.[14] Therefore the chemical formula can be written as $\{[Na_2(H_2O)_6][Mg(H_2O)_6][(SO_4)_2]\}\cdot 4H_2O$.

3.4. Comparison of the crystal structures

The quantitative comparison of the isotypic crystal structures within the $Na_2M(SO_4)_2\cdot 4H_2O$ series (M = Mg, V, Mn, Fe, Co, Ni, Zn, Cd) and between the two isotypic structures of $Na_2M(SO_4)_2\cdot 10H_2O$ (M = Mg, Ni), respectively was performed using

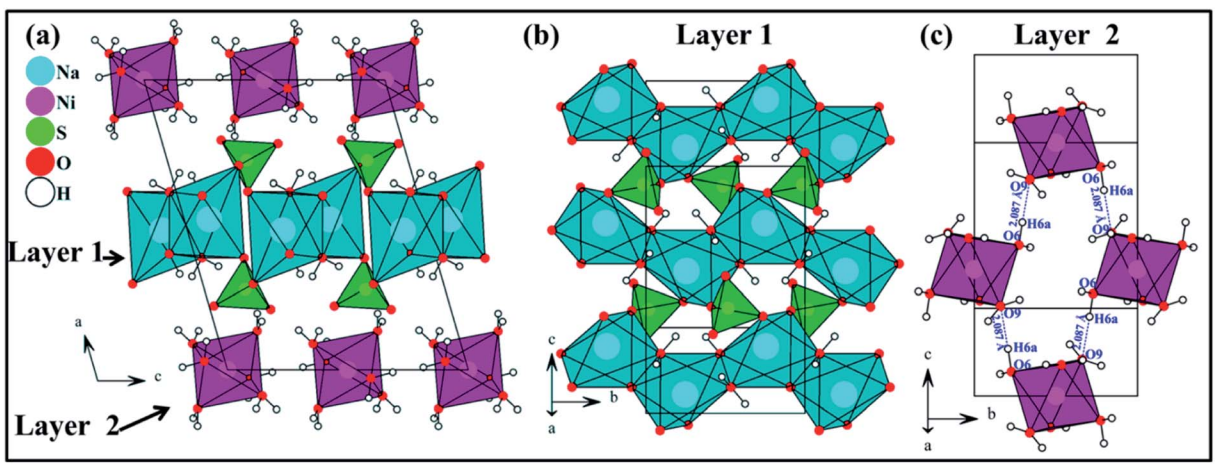

Fig. 8 View along the b axis of the crystal structure of $Na_2Ni(SO_4)_2\cdot 10H_2O$ (a), view of $[Na_2(SO_4)_2(H_2O)_4]^{2-}$ layer 1 on the (100) plane (b) and view of $[Ni(H_2O)_6]^{2+}$ layer 2 on the (100) plane (c).

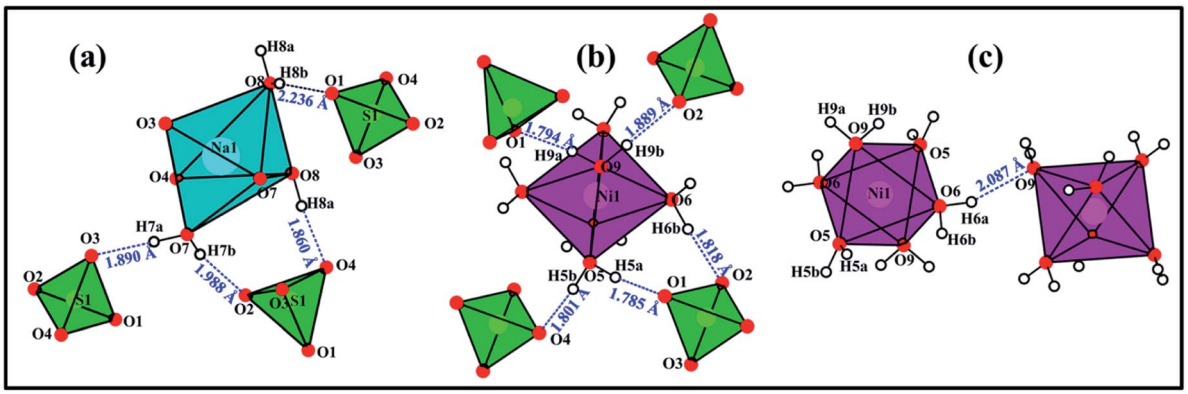

Fig. 9 View of the hydrogen bonds within the layer 1 (a), between layer 1 and layer 2 (b), and within the layer 2 (c).

the program compstru.[43–46] The comparisons did not include the hydrogen atoms since in the various structural refinements different constrains/restrains on the water molecules were applied. Origin shifts of $(0\ \frac{1}{2}\ \frac{1}{2})$ and $(0\ \frac{1}{2}\ 0)$ were applied to the crystal structures of $Na_2Mn(SO_4)_2\cdot 4H_2O$ and $Na_2Ni(SO_4)_2\cdot 10H_2O$, respectively. All the crystal structures in the $Na_2M(SO_4)_2\cdot 4H_2O$ series were compared to $Na_2Ni(SO_4)_2\cdot 4H_2O$ which was chosen as a reference. The numerical details of the comparisons are given in Table 5. The crystal structures of $Na_2Ni(SO_4)_2\cdot 4H_2O$ and its Mg, Fe, Co, and Zn analogues show a very high similarity ($\Delta < 0.02$) due to similar ionic radii of the five metal cations. Larger differences were observed with Mn and Cd ($\Delta = 0.044$ and 0.079, respectively) due to their greater ionic radii. It should be also noted that the cell volume increases almost linearly with the ionic radii of the metal cations (Fig. 11).

The crystal structure of $Na_2Ni(SO_4)_2\cdot 10H_2O$ was also compared to the Mg analogue using the compstru program. As indicated in Table 5, the two isotypic compounds are essentially coincident ($\Delta = 0.005$). The largest deviations of 0.0444 and 0.0430 were observed for the atom pairs O1 and O3 of the MgO_6 octahedron.

4. Conclusion

After the recent discovery of the new polymorphic modification of $Na_2Mn_3(SO_4)_4$ and the solid solution $Na_2Mn_{3-x}Mg_x(SO_4)$,[47] two other sulfate phases were prepared for the first time by a wet

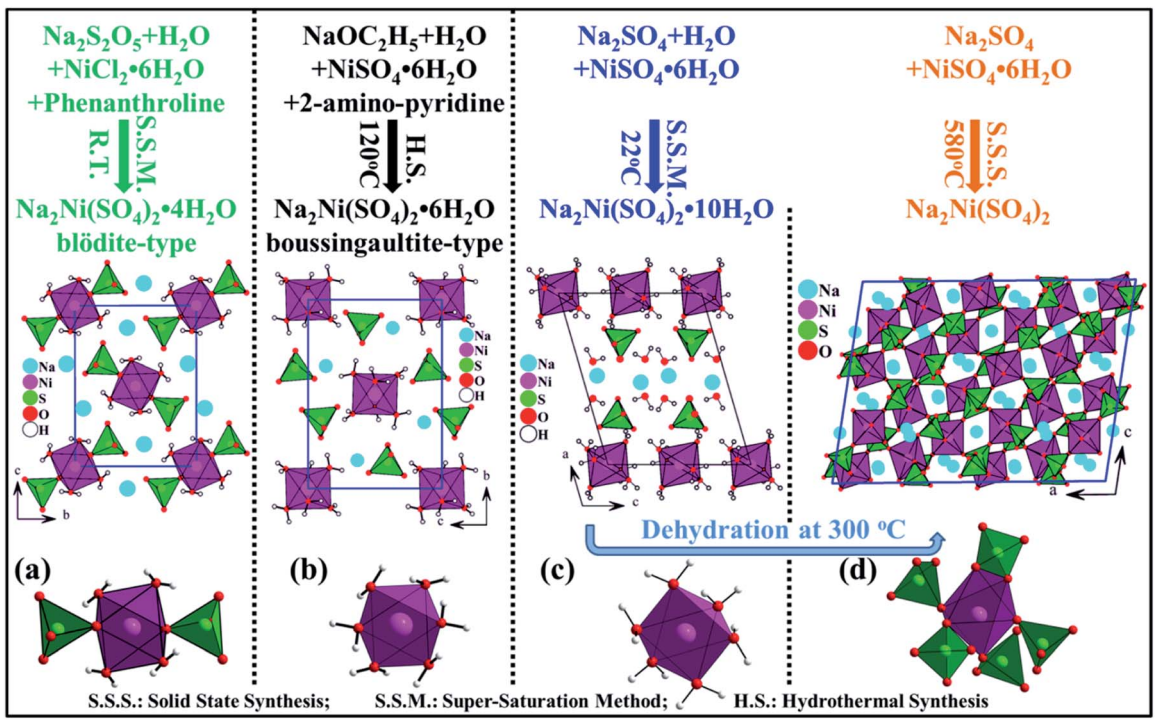

Fig. 10 Synthesis methods and crystal structure views for $Na_2Ni(SO_4)_2\cdot 4H_2O$ (a), $Na_2Ni(SO_4)_2\cdot 6H_2O$ (b), $Na_2Ni(SO_4)_2\cdot 10H_2O$ (c) and $Na_2Ni(SO_4)_2$ (d). The coordination spheres of the Ni atoms are also provided for comparison.

Table 5 Numerical details from the comparisons of the crystal structure of $Na_2Ni(SO_4)_2\cdot 4H_2O$ with isotypic structures in the $Na_2M(SO_4)_2\cdot 4H_2O$ series (M = Mg, V, Mn, Fe, Co, Ni, Zn, Cd), and between $Na_2Mg(SO_4)_2\cdot 10H_2O$ and $Na_2Ni(SO_4)_2\cdot 10H_2O$ using the compstru program (|*u*| is the atomic displacement)

$Na_2Ni(SO_4)_2\cdot 4H_2O$ *versus* $Na_2M(SO_4)_2\cdot 4H_2O$

M	Mg	Zn	Co	Fe	V	Mn	Cd
Atom	|*u*|/Å	|*u*|/Å	|*u*|/Å	|*u*|/Å	|*u*|/Å	|*u*|/Å	|*u*|/Å
Ni1/M	0.0000	0.0000	0.0000	0.0000	0.0000	0.0000	0.0000
Na1	0.0153	0.0088	0.0070	0.0091	0.0157	0.0285	0.0467
S1	0.0361	0.0197	0.0142	0.0241	0.0369	0.0523	0.0692
O1	0.0310	0.0216	0.0243	0.0505	0.0298	0.0626	0.0905
O2	0.0602	0.0172	0.0085	0.0226	0.0623	0.0325	0.0628
O3	0.0787	0.0320	0.0212	0.0343	0.0799	0.0797	0.1563
O4	0.0147	0.0183	0.0113	0.0115	0.0122	0.0456	0.1058
O5	0.0174	0.0228	0.0292	0.0580	0.0174	0.0965	0.1814
O6	0.0328	0.0337	0.0400	0.0719	0.0311	0.0971	0.1742
Degree of lattice distortion (S)	0.0034	0.0030	0.0030	0.0046	0.0057	0.0082	0.0138
The maximum distance (d_{max})/Å	0.0787	0.0337	0.0400	0.0719	0.0799	0.0971	0.1814
Arithmetic mean (d_{av})/Å	0.0337	0.0205	0.0183	0.0332	0.0336	0.0582	0.1043
Measure of similarity (Δ)	0.019	0.014	0.014	0.018	0.027	0.044	0.079
Ref.	7	7	7	34	33	This work	1

$Na_2Mg(SO_4)_2\cdot 10H_2O$ *versus* $Na_2Ni(SO_4)_2\cdot 10H_2O$

Atom	|*u*|/Å
Mg1/Ni1	0.0000
Na1	0.0117
S1	0.0217
O1	0.0444
O2	0.0220
O3	0.0430
O4	0.0210
O5	0.0132
O6	0.0242
O7	0.0181
O8	0.0094
O9	0.0377
Degree of lattice distortion (S)	0.0017
The maximum distance (d_{max})/Å	0.0444
Arithmetic mean (d_{av})/Å	0.0232
Measure of similarity (Δ)	0.005

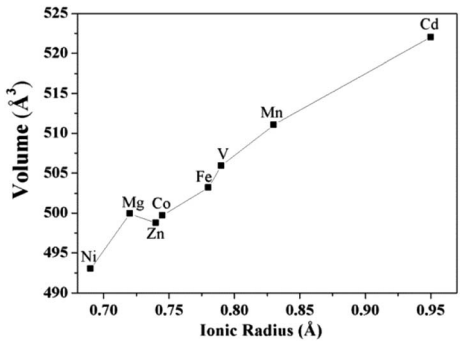

Fig. 11 Unit-cell volumes as a function of the ionic radius of the M cation in the blödite-type of compounds $Na_2M(SO_4)_2\cdot 4H_2O$ (M = Mg, V, Mn, Fe, Co, Ni, Zn, Cd).

chemistry route and their crystal structures were solved using single crystal XRD data. $Na_2Mn(SO_4)_2\cdot 4H_2O$ with the blödite-type structure is the missing link in the series of $Na_2M(SO_4)_2\cdot 4H_2O$ sulfates (M = Mg, V, Mn, Fe, Co, Ni, Zn, Cd), whereas $Na_2Ni(SO_4)_2\cdot 10H_2O$ is the first compound isostructural with the aristotype $Na_2Mg(SO_4)_2\cdot 10H_2O$. The powder XRD data revealed that only the nickel phase was almost pure, whereas the manganese phase was a mixture of at least three phases. The TGA data provided the optimal conditions to fully dehydrate the nickel phase. When $Na_2Ni(SO_4)_2\cdot 10H_2O$ is heated at temperatures between 300 and 600 °C, the anhydrous phase WC-$Na_2Ni(SO_4)_2$ could be obtained. Interestingly, it is isostructural with SS-$Na_2Ni(SO_4)_2$ which was prepared by solid state synthesis route and it is thermally more stable than $Na_2Fe(SO_4)_2$ which is a suitable cathode material for NIBs. Therefore, the dehydration of hydrous sulfates and phosphates should be considered as a promising step toward further realization of novel cathode materials for NIBs.

Conflicts of interest

The authors declare no conflict of interest.

Acknowledgements

Authors gratefully acknowledge financial support from National Priorities Research Program (NPRP9-263-2-122) funded by Qatar

National Research Fund (QNRF). Authors also would like to thank Dr Said Mansour for giving us access to the characterization tools in the core lab. The publication of this article was funded by the Qatar National Library.

References

1 D. K. Saha, G. Madras and T. N. Guru Row, *Cryst. Growth Des.*, 2011, **11**, 3213.
2 M. Wildner and D. Stoilova, *Z. Kristallogr.*, 2003, **218**, 201.
3 L. M. Dikareva, Y. V. Zefirov, A. N. Zhilyaev, I. B. Baranovskii and M. A. Porai Koshits, *Russ. J. Inorg. Chem.*, 1987, **32**, 64.
4 V. I. Bukin and Y. Z. Nozik, *J. Struct. Chem.*, 1974, **15**, 616.
5 M. Giglio, *Acta Crystallogr.*, 1958, **11**, 789.
6 M. E. Diaz Vivar, S. Baggio, A. Ibanez and R. F. Baggio, *Acta Crystallogr., Sect. E: Struct. Rep. Online*, 2008, **64**, i30.
7 D. Stoilova and M. Wildner, *J. Mol. Struct.*, 2004, **706**, 57.
8 P. Comodi, S. Nazzareni, T. Balic Zunic, A. Zucchini and M. Hanfland, *Am. Mineral.*, 2014, **99**, 511.
9 S. J. Mills, S. A. Wilson, G. M. Dipple and M. Raudsepp, *Mineral. Mag.*, 2010, **74**, 903.
10 E. M. S. Leduc, R. C. Peterson and R. Wang, *Am. Mineral.*, 2009, **94**, 1005.
11 W. Wu, J. M. Xie, D. P. Xie and Y. W. Xuan, *Acta Crystallogr., Sect. E: Struct. Rep. Online*, 2008, **64**, i7.
12 A. V. Kasatkin, F. Nestola, J. Plášil, J. Marty, D. I. Belakovskiy, A. A. Agakhanov, S. J. Mills, D. Pedron, A. Lanza, M. Favaro, S. Bianchin, I. S. Lykova, V. Goliáš and W. D. Birch, *Mineral. Mag.*, 2013, **77**, 367.
13 E. M. S. Leduc, R. C. Peterson and R. Wang, *Acta Crystallogr., Sect. C: Cryst. Struct. Commun.*, 2009, **65**, i81.
14 K. Leftwich, D. L. Bish and C. H. Chen, *Am. Mineral.*, 2013, **98**, 1772.
15 I. A. Trussov, L. L. Male, M. L. Sanjuan, A. Orera and P. R. Slater, *J. Solid State Chem.*, 2019, **272**, 157.
16 M. Reynaud, G. Rousse, A. M. Abakumov, M. T. Sougrati, G. Van Tendeloo, J. N. Chotard and J. M. Tarascon, *J. Mater. Chem. A*, 2014, **2**, 2671.
17 P. Singh, K. Shiva, H. Celio and J. B. Goodenough, *Energy Environ. Sci.*, 2015, **8**, 3000.
18 P. Barpanda, G. Oyama, C. D. Ling and A. Yamada, *Chem. Mater.*, 2014, **26**(3), 1297.
19 D. Swain and T. N. Guru Row, *Inorg. Chem.*, 2009, **48**, 7048.
20 D. Marinova, V. Kostov, R. Nikolova, R. Kukeva, E. Zhecheva, M. Sendova-Vasileva and R. Stoyanova, *J. Mater. Chem. A*, 2015, **3**, 22287.
21 P. Barpanda, G. Oyama, S. Nishimura, S.-C. Chung and A. Yamada, *Nat. Commun.*, 2014, **5**, 4358.
22 G. Oyama, S. Nishimura, Y. Suzuki, M. Okubo and A. Yamada, *ChemElectroChem*, 2015, **2**, 1019.
23 G. Oyama, O. Pecher, K. J. Griffith, S. Nishimura, R. Pigliapochi, C. P. Grey and A. Yamada, *Chem. Mater.*, 2016, **28**, 5321.
24 A. M. Fry, O. T. Sweeney, W. A. Phelan, N. Drichko, M. A. Siegler and T. M. McQueen, *J. Solid State Chem.*, 2015, **222**, 129.
25 M. E. D. De Vivar, S. Baggio, M. T. Garland and R. F. Baggio, *Acta Crystallogr., Sect. E: Struct. Rep. Online*, 2006, **62**, i196.
26 P. S. Zhao, F. F. Jian, Z. S. Bai, J. Zheng and R. R. Zhuang, *Struct. Chem.*, 2006, **17**, 519.
27 V. Petricek, M. Dusek and L. Palatinus, Crystallographic Computing System JANA2006: General features, *Z. Kristallogr.*, 2006, **229**, 345.
28 Bruker, *APEX3, SAINT and SADABS*, Bruker AXS Inc., Madison, Wisconsin, USA, 2016.
29 L. Palatinus and G. Chapuis, *J. Appl. Crystallogr.*, 2007, **40**, 786.
30 E. Matzat, *Neues Jahrb. Mineral., Abh.*, 1970, **113**, 1.
31 A. V. Kasatkin, M. Favaro, S. Bianchin, I. S. Lykova, V. Golias, W. D. Birch, F. Nestola, J. Plasil, J. Marty, D. I. Belakovskiy, A. A. Agakhanov, S. J. Mills, D. Pedron and A. Lanza, *Mineral. Mag.*, 2013, **77**, 367.
32 I. M. Rumanova, *Dokl. Akad. Nauk SSSR*, 1958, **118**, 84.
33 S. Peytavin and L. Cot, *C. R. Seances Acad. Sci., Ser. C*, 1969, **269**, 1206.
34 M. Hudak, J. G. Diaz and J. Kozisek, *Acta Crystallogr., Sect. E: Struct. Rep. Online*, 2008, **64**, i10.
35 E. H. Nickel and P. J. Bridge, *Mineral. Mag.*, 1977, **4137**, 41.
36 J. Schlueter, K.-H. Klaska and G. Gebhard, *Neues Jahrb. Mineral., Monatsh.*, 1999, **3**, 97.
37 D. Marinova, M. Wildner, T. Bancheva, R. Stoyanova, M. Georgiev and D. G. Stoilova, *Phys. Chem. Miner.*, 2018, **45**, 801.
38 R. D. Shannon, *Acta Crystallogr., Sect. A: Cryst. Phys., Diffr., Theor. Gen. Crystallogr.*, 1976, **32**, 751.
39 I. D. Brown and D. Altermatt, *Acta Crystallogr., Sect. B: Struct. Sci.*, 1985, **41**, 244.
40 T. Steiner, *Angew. Chem., Int. Ed.*, 2002, **41**, 48.
41 G. A. Jeffrey, *An Introduction to Hydrogen Bonding*, Oxford University Press, Oxford, 1997.
42 D. Dwibedi, R. B. Araujo, S. Chakraborty, P. P. Shanbogh, N. G. Sundaram, R. Ahuja and P. Barpanda, *J. Mater. Chem. A*, 2015, **3**, 18564.
43 G. de la Flor, D. Orobengoa, E. Tasci, J. M. Perez-Mato and M. I. Aroyo, *J. Appl. Crystallogr.*, 2016, **49**, 653.
44 C. Capillas, J. M. Perez-Mato and M. I. Aroyo, *J. Phys.: Condens. Matter*, 2007, **19**, 275203.
45 D. Orobengoa, C. Capillas, M. I. Aroyo and J. M. Perez-Mato, *J. Appl. Crystallogr.*, 2009, **42**, 820.
46 G. Bergerhoff, M. Berndt, K. Brandenburg and T. Degen, *Acta Crystallogr., Sect. B: Struct. Sci.*, 1999, **55**, 147.
47 H. Ben Yahia, *Z. Kristallogr.–Cryst. Mater.*, 2019, **234**, 697.

